

# COMMISSIONING OF THE UCLA NEPTUNE X-BAND DEFLECTING CAVITY AND APPLICATIONS TO CURRENT PROFILE MEASUREMENT OF RAMPED ELECTRON BUNCHES\*

R. J. England, B. O’Shea, J. B. Rosenzweig, G. Travish, UCLA, Los Angeles, CA 90095, USA  
 D. Alesini, INFN/LNF, Frascati, Italy

## Abstract

A 9-cell standing-wave deflecting cavity has recently been constructed and installed at the UCLA Neptune Laboratory for use as a temporal diagnostic for the 13 MeV, 300 to 700 pC electron bunches generated by the Neptune photoinjector beamline. The cavity is a center-fed Glid-Cop structure operating in at  $TM_{10}$ -like deflecting mode at 9.59616 GHz with a  $\pi$  phase advance per cell. At the maximum deflecting voltage of 530 kV, the theoretical resolution limit of the device is 50 fs, although with current beam parameters and a RMS spot size of 460  $\mu\text{m}$  the effective resolution is approximately 400 fs. We discuss the operation and testing of the cavity as well as its intended application of measuring the temporal current profile of ramped electron bunches generated using the Neptune dogleg compressor, and we present the first measurements of the electron beam current profile obtained using the deflecting cavity.

## INTRODUCTION

We recently proposed a scheme for generating relativistic electron bunches having a triangular or ramp-shaped current profile (i.e. rising linearly from head to tail and then dropping sharply to zero) and initiated an experiment to test this technique at the UCLA Neptune linear accelerator laboratory [4]. A triangularly ramped bunch approximates the so-called "doorstep" profile which has been predicted by both 1D and 2D plasma theory to be an ideal shape for the drive beam in a plasma wakefield accelerator (PWFA) [1, 2, 3], as it maximizes the *transformer ratio*, which is a figure of merit for the PWFA, defined by  $R = E_+/E_-$  where  $E_+$  is the peak accelerating field behind the bunch and  $E_-$  is the peak decelerating field within the bunch.

The proposed method for generating the ramped bunches is discussed in detail in Ref. [4]. In short, the technique requires injecting an electron bunch with a positive energy chirp (i.e. particles at the head of the bunch are at higher energy) into a dogleg, or dispersionless translating section, which serves as a bunch compressor. A cartoon of the experimental beamline is shown in Fig. 1. The bunch-shaping mechanism is dependent upon the  $z$  phase space transformation being *linear* (i.e. dominated by the linear longitudinal dispersion term or  $R_{56}$  in transport notation). However, since a chirped beam injected off-crest tends to have

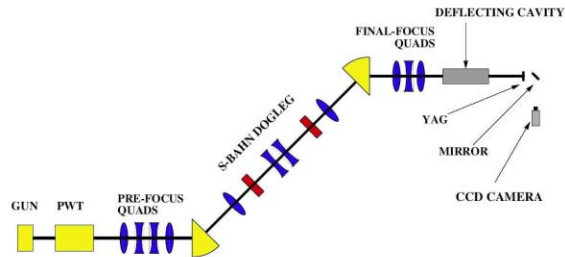


Figure 1: Cartoon drawing of experimental beamline.

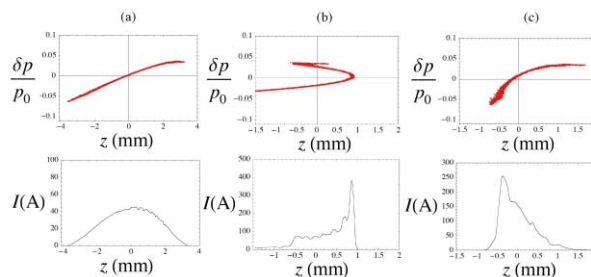


Figure 2: Plots showing (a) an initially chirped distribution in longitudinal phase space which has been artificially manipulated by imposing the simple transformation of Eq. 1 with (b) both the  $R_{56}$  and  $T_{566}$  terms included and (c) only the  $R_{56}$  term included.

a larger energy spread, the longitudinal dispersion contains a significant second-order contribution. The longitudinal transport to second order is therefore approximated by

$$z_f \approx z_0 + R_{56}\delta + T_{566}\delta^2, \tag{1}$$

where  $z_0$  and  $z_f$  are the initial and final longitudinal coordinates of a test particle and  $\delta = \Delta p/p_0$  is the momentum error. The second-order contribution to the longitudinal dispersion is represented by the transport matrix element  $T_{566}$ . Elimination of the  $T_{566}$  contribution is accomplished by the use of sextupole corrector magnets, shown as red rectangles in Fig. 1.

The fundamental bunch-shaping mechanism is illustrated in Fig. 2, where an initially chirped distribution of particles in longitudinal phase space, shown in part (a), has been artificially manipulated by applying the transformation of Eq. 1 to each particle in the distribution. In part (b) both the linear and quadratic terms have been included

\* Work supported by U.S. Department of Energy under Grant No. DE-FG03-92ER40693

(with values of  $R_{56}$  and  $T_{566}$  similar to those of the actual beamline) whereas in (c) only the linear  $R_{56}$  term is included. We see in part (c) that the linearized transformation in conjunction with the intrinsic RF curvature of the initial distribution produces a “hook-shaped” distribution with a ramp-shaped current profile.

Experimental measurements of the post-compression bunch length, obtained by coherent transition radiation (CTR) interferometry, as a function of sextupole strength have been reported previously and compared favorably with simulations using the particle tracking codes PARMELA and ELEGANT [4]. However, CTR interferometry does not provide detailed information about the longitudinal shape of the electron bunch. Consequently, a transverse deflecting mode cavity was designed and built as a temporal diagnostic capable of resolving the temporal structure of the sub-picosecond to several picosecond duration electron bunches generated by the Neptune linear accelerator beamline and dogleg compressor. When a beam is injected into such a cavity at the zero-crossing of the RF, it experiences a transverse momentum kick along the orthogonal transverse axis whose strength is approximately linear in the arrival time of the particles. As a result, the longitudinal distribution of the beam is deflected transversely and can be imaged on a simple profile monitor located downstream (see e.g. Ref. [5]).

## DEFLECTING CAVITY DESIGN

The deflecting cavity which was recently built and commissioned for use in the Neptune laboratory is a 9-cell standing-wave structure, operating in a  $TM_{110}$ -like dipole mode. The cavity design is distinguished by a number of unique features. These include the high (X-Band) operating RF frequency of 9.59616 GHz, low input power requirement (50 kW), and the use of a knife-edge conflat-style vacuum seal machined directly into the mating faces of the cells, which allows the cavity to be easily disassembled and eliminates the need for brazing or welding, which can warp and detune the cells. The cavity material was chosen to be GlidCop Al-15. A drawing of the assembled prototype cavity is shown in Fig. 3 with a quarter section removed to reveal the interior of the structure. The 9-cell structure was designed in three phases (with two prototypes) using the commercial RF modeling code HFSS 9.2. A list of simulated and measured parameter values are shown in Table 1.

The temporal resolution limit due to the camera and optics used to image the final screen is approximately 50 fs. However the achievable temporal resolution of the deflecting cavity was found to be limited by the minimum spot size  $\sigma_0$  that can be achieved on the downstream imaging screen when the cavity is turned off to a value of approximately 400 fs at the maximum cavity voltage of 530 kV.

A bead pull was performed using an uncalibrated aluminum bead. The resulting shift in frequency as a function of the bead position along the cavity axis (Fig. 4) was mea-

Table 1: Measured and Simulated Cavity Parameters

Parameter	Measured	HFSS	Units
Number of Cells	9	9	-
Pi-Mode Freq	9.59616	9.60084	GHz
Deflecting Voltage	0-530	528	kV
Quality Factor	13043	13672	-
Cell Radius	18.25	18.25	mm
Cell-to-Cell Distance	15.62	15.62	mm
Iris diameter	10	10	mm
Beam pipe diameter	10	10	mm
VSWR	1.04	1.028	-

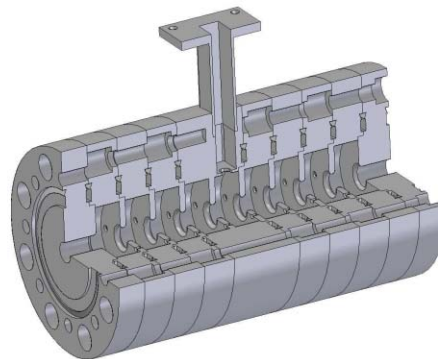


Figure 3: Cutaway drawing of the assembled 9-cell cavity design.

sured using a network analyzer. The frequency shift for a spherical bead is related to the field amplitudes  $E_0$  and  $H_0$  along the axis by the formula  $\Delta f/f_0 = \pi a^2(|E_0|^2 - \frac{1}{2}|H_0|^2)/W_0$ , where  $a$  is the bead diameter, and  $W_0$  is the stored energy in the cavity [6]. Consequently, the positive peaks in Fig. 4 correspond with the irises where  $E_0$  is maximum, and the negative peaks correspond with the centers of the cells where  $H_0$  is maximum. The field imbalance appears magnified by the dependence of the plot on the square of the fields  $|E_0|^2$  and  $|H_0|^2$ . However, taking the square roots of the magnitudes of the positive and negative peaks gives a maximum variation in cell-to-cell field strength of only 10%.

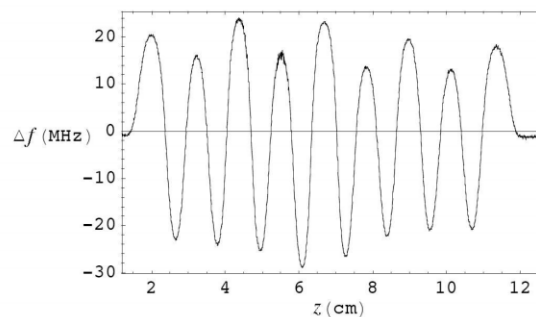


Figure 4: Bead pull field measurement of the deflecting cavity using a metallic bead.

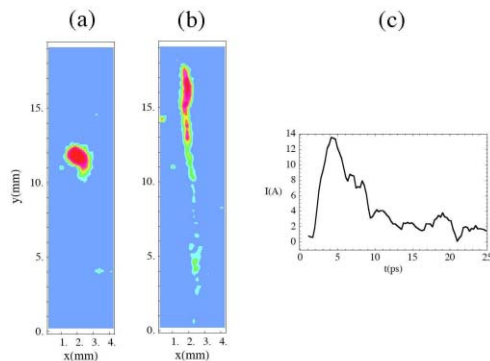


Figure 5: Deflecting cavity streaks of the uncompressed bunch with (a) deflecting cavity off, (b) deflecting cavity on, and (c) the reconstructed current profile.

## ELECTRON BUNCH PROFILE MEASUREMENTS

The bunch-shaping scheme for generating ramp-shaped electron bunches proposed in Ref. [4] relies upon injecting an electron beam that has been given a positive energy chirp in the linac (i.e. higher energy particles are at the head of the beam) into the sextupole-corrected dogleg compressor shown in Fig. 1. For an unchirped beam (i.e. on-crest in the linac), there is no significant compression in the dogleg section and the deflecting cavity streak measures the current profile of the uncompressed bunch. An example streak is shown in Fig. 5, indicating an asymmetrical longitudinal bunch shape, presumably inherited from the temporal shape of the UV photocathode drive laser pulse. The extracted RMS bunch length  $\sigma_t = 5.9$  ps extracted from this plot is consistent with an estimate of the photocathode laser pulse length at the cathode derived from autocorrelation interferograms of the drive laser pulse.

Streaks taken with bunches chirped in the linac by choosing the injection phase to lie approximately 15 degrees back-of-crest, are shown in Fig. 6 for five different sextupole field strengths, along with corresponding current profile reconstructions. The slight horizontal tilt to the streaks is the result of a residual horizontal dispersion introduced by detuning of one of the dogleg quadrupole magnets. The result is a partial reconstruction of the longitudinal phase space, with the horizontal and vertical axes on the streak image representing energy and time respectively. This permits a visualization of the phase space transformation taking place as the sextupole field strength is varied. From the reconstructed current profiles, we see that the initial shape of the bunch in Fig. 6(a) resembles the prediction of our simple model in Fig. 2(b) and progresses toward a ramped distribution as the sextupole field is increased, and the nonlinear term  $T_{566}$  in Eq. 1 is reduced. It should be noted, however that the sextupole field value corresponding to  $T_{566} = 0$  lies intermediate between the values corresponding to Fig. 6(c) and 6(d). Therefore, the ramped bunch shown in Fig. 6(e) is produced by overcompensat-

06 Instrumentation, Controls, Feedback & Operational Aspects

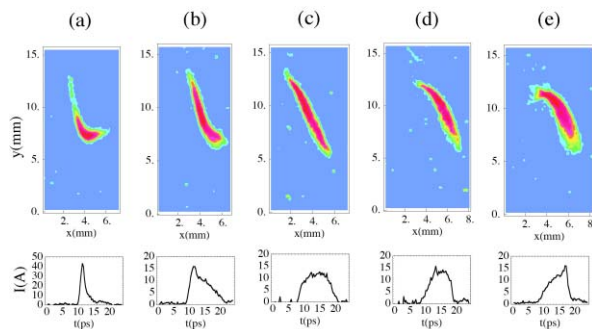


Figure 6: Deflecting cavity streaks and reconstructed current profiles of the (234 pC, 11.86 MeV) compressed bunch at sextupole field strength values of (a)  $\kappa = 0$ , (b)  $\kappa = 547 \text{ m}^{-3}$ , (c)  $\kappa = 1094 \text{ m}^{-3}$ , (d)  $\kappa = 1641 \text{ m}^{-3}$ , and (e)  $\kappa = 2188 \text{ m}^{-3}$ .

ing with the sextupoles, reversing the sign of the  $T_{566}$  and thereby reinforcing the hard-edged cutoff at the tail of the beam. This overcompensation is required due to the asymmetrical initial (pre-compression) bunch shape and slightly nonoptimal linac injection phase.

## CONCLUSIONS

The UCLA Neptune deflecting cavity has been built, installed, tested, and found to operate well within specifications. The cavity has been used successfully to reconstruct the current profiles of electron bunches produced by the Neptune linear accelerator and dogleg compressor with approximately 400 fs resolution, and the results are consistent with the mechanism for generating ramp-shaped electron bunches which was proposed in Ref. [4].

## REFERENCES

- [1] K. L. F. Bane, Pisin Chen, and P. B. Wilson. On Collinear Wake Field Acceleration. Technical Report SLAC PUB-3662, Stanford Linear Accelerator Center, Stanford, CA 94305, April 1985.
- [2] J. B. Rosenzweig. Acceleration and focusing of electrons in two-dimensional nonlinear plasma wake fields. *Phys. Rev. A*, 44:R6189–6192, November 1991.
- [3] K. V. Lotov. Efficient operating mode of the plasma wakefield accelerator. *Physics of Plasmas*, 12:053105, 2005.
- [4] R. J. England, J. B. Rosenzweig, G. Andonian, P. Musumeci, G. Travish, and R. Yoder. Sextupole Correction of the Longitudinal Transport of Relativistic Beams in Dispersionless Translating Sections. *Phys. Rev. ST-AB*, 8:12801, January 2005.
- [5] G. A. Loew and O. H. Altenmueller. Design and Application of RF Separator Structures at SLAC. Technical Report PUB-135, Stanford Linear Accelerator Center, Stanford, CA, 1965.
- [6] J. C. Slater. *Microwave Electronics*. Van Nostrand, Princeton, NJ, 1950.

T03 Beam Diagnostics and Instrumentation